Int. J. Nano Dimens., 15 (1): 1-22, Winter 2024

ORIGINAL ARTICLE

Chemical synthesis of Lead Iodide nanoparticles for photovoltaic and optoelectronic device applications

Madhavi Sharad Darekar, Praveen Beekanahalli Mokshanatha*

Department of Physics, Institute of Engineering and Technology, Srinivas University, Mukka, Surathkal, Mangalore- 574146, Karnataka, India

Received 29 September 2023, revised 28 October 2023, accepted 06 November 2023, available online 10 November 2023

Abstract

In the present study, the highly recommended lead iodide (PbI_2) nanoparticles and thin films based on PbI_2 nanoparticles have been prepared for optoelectronics and solar cell applications. PbI_2 is an anisotropic p-type semiconductor with a band gap of 2.57 eV at room temperature. PbI_2 material has large potential applications in optical detector, digital X-ray imaging, gamma ray detector, etc. PbI_2 layered semiconductor nanoparticles were stabilized using thioglycerol and investigated by Ultraviolet-Visible (UV-Vis) absorption spectroscopy, X-ray Diffraction (XRD), X-ray Photoelectron Spectroscopy (XPS), transmission electron microscopy (TEM) and photoluminescence (PL) spectroscopy. The chemical bath deposition (CBD) method was used to deposit PbI_2 thin films on fluorine-doped tin oxide (FTO) glass substrates. These films were characterized by scanning electron microscopy (SEM), energy-dispersive X-ray spectroscopy (EDX), mapping and atomic force microscopy (AFM). The thicknesses of the PbI_2 thin films were estimated using a laser profilometer. The blue shift was observed in UV-Vis absorption and PL spectra of PbI_2 nanoparticles. TEM was used to obtain quantitative information on the PbI_2 particle size distribution. Due to the low solubility of PbI_2 in acetonitrile, approximately 20-30 nm sized circular particles are obtained. The variation of 18 Å was observed in the lateral dimensions of PbI_2 nanoparticles. Pb4fXPS core level appeared at 138.5 eV corresponding to PbI_2. There is no report published wherein the PbI_2 nanoparticles and the PbI_2 thin films were prepared by the aqueous chemical method and the CBD method respectively. In this study, the characterization results of PbI_2 nanoparticles and PbI_2 thin films were better than many other materials.

Keywords: *Characterization; Chemical Bath Deposition Method; Nanoparticles; PbI_2 Thin Films; Synthesis.*

How to cite this article

Sharad Darekar M., Beekanahalli Mokshanatha P., Chemical synthesis of Lead Iodide nanoparticles for photovoltaic and optoelectronic device applications. Int. J. Nano Dimens., 2024; 15(1): 1-22.

INTRODUCTION

The size quantization effect observed in case of semiconductor nanoparticles [1-6] has led to numerous efforts to populate the particles of certain sizes. A number of methods have been used to synthesize nanoparticles with narrow size distribution. There are many examples of IV group, I-VI group, II-VI group and III-IV group semiconductors where this has been possible to a more or less good extent. Although in many cases colloidal particles suspended in liquids were investigated for their optical properties, the applications require the particles in the form of powder or thin films. However, in the case of PbI_2, colloids are often synthesized or mixtures of various sizes have been produced. For obtaining the aforementioned forms of PbI_2 particles, some of the routinely used methods are chemical capping, use of zeolites, glass matrix, polymer coating etc.

There is a lot of interest in synthesizing nanoparticles of narrow size distribution so as to exploit their size dependent properties. In semiconductor nanoparticles, when the size of the particles is similar to or less than the size of the Bohr diameter for the exciton, the energy gap begins to widen and a greater excitonic peak becomes visible even at room temperature [7, 8]. The particle size decreases and the energy gap increases with an

* Corresponding Author Email: *madhavi_darekar28@rediff.com*

increase in the concentration of the capping agent in case of semiconductor nanoparticles [4-6]. This provides an opportunity to fabricate novel optoelectronic devices. Interestingly, a variety of methods of synthesis can be utilized to obtain nanoparticles in different media like glasses, zeolites, polymers etc. and avoid expensive routes of bottom down technology. Synthesis of layered semiconductor nanoparticles like PbI_2, HgI_2, CdI_2, BiI_3 has been carried out in the past [9-11].

PbI_2 is a IV-VII group p-type semiconductor having a band gap of 2.57 eV [12, 13] at room temperature. In the PbI_2 layered semiconductor with its band structure, the layer of lead ions is sandwiched between two layers of iodine ions that are packed closely and hexagonally [10, 14-17]. The layers of lead and iodine atoms are perpendicular to the c-axis and they are held together by van der Waals forces [10, 13, 16, 18]. For PbI_2 semiconductor nanoparticles to exhibit the quantum size effect, the particle size should be comparable to or smaller than 3.8 nm because the Bohr radius of exciton for PbI_2 is 1.9 nm [10]. PbI_2 is an anisotropic [10, 13] semiconductor which crystallizes in the CdI_2 type of layer structure [18]. PbI_2 shows interesting optical [18, 19], photoconductive and electronic properties [10, 12, 13]. The other properties of PbI_2 are thermal stability, lower vapor pressure [12], two-dimensional layered structure, band-gap in the visible range (2.30 eV) and high molar mass [15]. Transport properties of PbI_2 layered semiconductor at high electric fields along the c-axis were determined by R. Minder et al. [20]. PbI_2 material has potential applications like solar cells, optical detectors, X-ray radiation detectors, γ-ray detector (due to high atomic number of Pb – 82, and I – 53), digital X-ray imaging, photo-optical devices etc. at room temperature with high efficiency due to wide band gap [12-15, 21-23]. The size dependent optical and electrical properties are observed in PbI_2 nanoparticles due to the quantum size effect. Due to the size dependent physical characteristics [12], PbI_2 semiconductor nanoparticles have large commercial applications in X-ray digital radiography detectors, co-precipitation sensors, photo detectors, sensors, photo-catalysis, lubrication, nonlinear optics, biological labeling and diagnostics, photo-electrochemistry [24] and light emitting diodes (LED) including photo-electro-co-precipitation solar cells [13, 16, 22, 24]. PbI_2 has been the subject of much attention lately because of its capacity to react with amine iodides, including methyl ammonium iodide (CH_3NH_3I–MAI). These reactions produce materials with extraordinary optoelectronic properties, halide perovskites like $CH_3NH_3PbI_3$ (MAPI), which are used in high efficiency perovskite solar cells (PSC). PSCs have used atomic layer deposition (ALD) to deposit metal oxides that act as charge carrier blocking, junction creating, or encapsulating layers. On the other hand, because halide perovskites and metal iodides lack ALD processes, ALD is still poorly understood in the context of halide perovskites [15]. ALD can coat structures with a high aspect ratio (HAR), it works well with roll-to-roll manufacturing, and makes composition control in multicomponent films simple. Regarding halide perovskite devices, these characteristics are important. Though roll-to-roll production has promise for flexible halide perovskite photovoltaics and light emitting diodes, covering HAR structures can be helpful for producing halide perovskite films for transistors. The ability to tune the electrical and optical characteristics of the perovskites makes composition control essential for all halide perovskite applications [15]. PbI_2 is used as a precursor of the hybrid organic/inorganic active material in perovskite solar cells, $MAPbI_3$, where MA is the methyl-amide group [13]. This has led to a recent resurgence of interest in PbI_2 due to the developing field of organometal trihalide perovskite photographic solar cells.

In case of PbI_2, most of the attempts have been made to synthesize them as colloids suspended in liquids (acetonitrile) where they can remain separated due to electrostatic interaction. The PbI_2 particles should be stabilized using some surface-active agent or encapsulated in some stable matrix like polymer, zeolite or glass to avoid the coalescence of nanoparticles and maintain their size dependent properties. In the past, the PbI_2 nanoparticles embedded in zeolite [25] and silica glass [10] have been synthesized. We have demonstrated that it is indeed possible to use organic molecules like thioglycerol to passivate the PbI_2 particles. This method has an advantage of producing dry powder of PbI_2 to make pellets or solution containing PbI_2 in thioglycerol, and may be utilized for preparing thin film by spin coating, dip coating or chemical bath deposition methods.

Previously, various methods like chemical method [14], sol-gel method [10], co-precipitation method, microwave irradiation method,

hydrothermal method [26, 27] etc. were used to synthesize PbI_2 nanoparticles. However, in majority of the attempts, PbI_2 nanoparticles were synthesized as colloids in some organic liquids. The electrostatic interaction between the particles controls the particle growth in solutions. However, the surfaces of the particles must be passivated to employ them as dry powders or thin films. As the chemical method is simple, less expensive, easily available and easily accessible, it is widely used to synthesize the nanoparticles as compared to any other method. Using chemical synthesis methods, nanoparticles can be produced as colloids and then stabilized with some procedural modification. It is also possible to form thin films of stabilized nanoparticles without altering their particle size.

Various techniques like chemical vapour deposition [28], vacuum evaporation [29], pulsed laser deposition [30], electro-chemical deposition [31], vacuum sublimation [32], spin coating [33], spray pyrolysis [34], thermal evaporation method [13, 24] and atomic layer deposition (ALD) [15] were used for deposition of PbI_2 thin films. CBD technique depends on the immersion of the FTO glass slide into the precursor solution containing cations and anions [35]. CBD is a very simple, non-polluting, inexpensive [36] and convenient method used for making good quality, uniform, homogeneous and large area thin films [37] for industrial scale [38]. Thin film deposition is performed by precipitation using a controlled chemical reaction in CBD method [39]. The best photoconductivity and morphological properties such as surface roughness and pinhole density are obtained in CBD deposited thin films [40, 41]. It is not necessary to have a high temperature, high pressure or vacuum system [42] in CBD process which makes it a preferable method in comparison with the other methods [43]. Eco-friendly procedure is used in CBD technique [44]. Only the precursor solution, containers and substrate mounting devices are needed for the CBD method, which makes it better than other methods. There is nucleation and particle growth in the CBD process which forms a solid from the solution [45]. The optical, structural and electrical properties of the CBD deposited thin films are affected by the deposition temperature, pH of solution, deposition time, molarities and chemical reagents [38, 42, 45]. The economical CBD method produces stable, adherent, uniform and hard films with good reproducibility. The growth conditions such as deposition time, composition, solution temperature, topographical, and chemical nature of the slide are dependent on the film thickness [45].

In this study, the aqueous chemical method was used to stabilize thioglycerol capped PbI_2 layered semiconductor nanoparticles at room temperature. It was possible to obtain the nano-sized, mono-dispersed PbI_2 particles by increasing the concentration of the stabilizer. Use of different stabilizing chemicals and their concentrations have profound effect on the morphology of the resulting aggregates. UV-Vis absorption, XPS and TEM were performed to investigate PbI_2 nanoparticles. The CBD method was used to deposit the PbI_2 thin films on FTO glass slides. These films were analysed by XRD, SEM, EDAX, mapping and AFM.

Previously, several characterization techniques were used extensively to characterize the PbI_2 nanoparticles, the results of which indicate that the physical properties of these nanoparticles have changed drastically compared with the bulk PbI_2 material and such nanoparticles were utilized in different technological applications. We have obtained similar results with pure PbI_2 nanoparticles.

We have demonstrated that PbI_2 particles can be passivated using short chain organic or inorganic molecules. Synthesis of the particles can be carried out in a solution but stable dry powders can be obtained with particles in the narrow size regions. We have compared our results with the PbI_2 nanoparticles synthesized by other researchers. Thermal stability of the passivation is also discussed.

The aim of the present work is to discuss about the synthesis of the PbI_2 nanoparticles using the aqueous chemical method, preparation of PbI_2 thin films by the CBD method, and their characterization results. Synthesis and investigation of nanoparticles is considered to be a difficult task as compared to the bulk material. Such nanoparticles embedded in solid matrix are useful for a variety of applications. The optical, structural and electrical properties of PbI_2 nanoparticles have also been discussed in more detail.

MATERIALS AND METHODS

Based on the science of low dimensional materials, nanotechnology has been considered to be the leading technology of the twenty

first century. It is expected that electronics, optoelectronics, automobiles, medicines, sports goods etc. are using nanomaterials invading all walks of our lives. Therefore, there is a lot of enthusiasm amongst the scientists to synthesize, organize and characterize low dimensional materials.

When one, two or all three dimensions of a material reduce below ~ 100 nm size, it is known as a thin film, a wire or a dot respectively. At such a size, the scale properties of metals, semiconductors or insulators are predominantly size dependent. Due to this, it is possible to tailor the properties making it colourful or colourless, transparent or opaque, magnetic or nonmagnetic, and so on, without altering the chemical formula (or stoichiometry of the constituents) of the nanomaterials. However, it is quite important at this stage to understand the properties of novel nanomaterials.

As nanoparticles are characterized by size dependent properties, it is necessary to obtain the narrow size distribution. The undoped PbI_2 nanoparticles with a size less than or comparable to Bohr diameter of exciton have been synthesized by the chemical method. Especially, the chemical method works extremely well for the synthesis of IV-VII group semiconductors because of several advantages. Chemical method is a relatively simple and inexpensive approach to synthesize the nanoparticles and has been adopted even in the past. There are many examples of IV group, I-VI group, II-VI group semiconductors wherein the particles with narrow size distribution are obtained [1-6, 46]. Different capping agents and media may be used for the synthesis of nanoparticles. However, in this work, thioglycerol [$SHCH_2CH(OH)CH_2OH$] has been used to passivate the particle surface [4- 6].

There are different characterization techniques which can be used to analyze the nanoparticles. UV-Vis absorption is the simplest method to understand the formation of nanoparticles with quantum confinement. The electronic properties can be studied and also the surface and bulk defects can be determined by using the photoluminescence technique [4-6]. Structural analysis of nanoparticles is a challenging job because nanoparticles are often very small (~ 1 nm diameter) containing only few tens of atoms. Therefore, periodicity of bulk solids is not well developed. The XRD technique is widely used to determine the size measurements of the nanoparticles and also their phase [4-6]. The XPS method checks the presence of impurity in nanoparticles. The SEM technique determines the size distribution of the nanoparticles. The presence of the elements in nanoparticles is given in atomic percentages by EDX. The quantitative information on the distribution of crystallites, the particle sizes and the growth pattern are obtained by analysing the nanoparticles by TEM. The surface morphology of the PbI_2 thin films was analyzed by the AFM study [4-6].

Experimental Procedure for The Synthesis of PbI_2 Nanoparticles

The synthesis of PbI_2 nanoparticles of different sizes was done by the aqueous chemical method at room temperature at varying concentrations of thioglycerol. The flow chart for the preparation of PbI_2 particles (sample A) is shown in Fig. 1. The aqueous solution of the starting material $Pb(NO_3)_2$ (0.01 M in 25 ml DDW) was stirred in the reaction vessel using a magnetic stirrer. Then the aqueous solution of thioglycerol (0.8 M in 25 ml DDW) was added drop wise to $Pb(NO_3)_2$ by an equalizer. Finally, the aqueous solution of the starting material KI (0.05 M in 25 ml DDW) was added into the reaction vessel and the whole solution was stirred under nitrogen atmosphere. Double distilled or deionised water was used as the solvent in solution preparations. In reaction process, it makes no difference either to start with $Pb(NO_3)_2$ or KI. The only important factor is the addition of the capping agent which should be in between the additions of the starting materials $Pb(NO_3)_2$ and KI. The experiments were carried out at room temperature (30 °C) under nitrogen atmosphere. The final colloidal solution was centrifuged and the precipitate was washed 3-4 times with double distilled water. The precipitate was transferred to Petri dish and air dried to get the PbI_2 nanoparticles (sample A). The similar procedure was followed to synthesize the PbI_2 nanoparticles (sample B) by using the thioglycerol concentration of 0.001 M.

The nucleation is rapid when the chemical reaction between the lead nitrate and potassium iodide is rapid. The growth process depends on the rate of nuclei production. The autocatalytic growth increases rapidly with increased nucleation, and with increased nucleation, a large number of small sized particles are formed. Slow

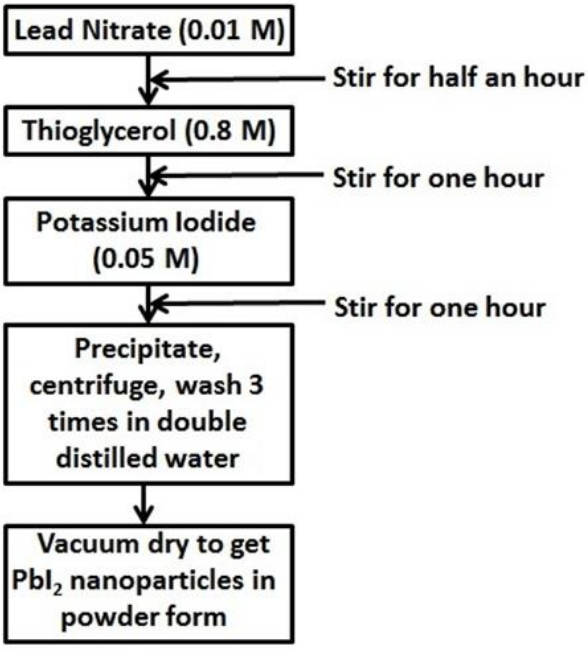

Fig. 1. Flow chart for the preparation of PbI_2 particles (sample A).

Table 1. Bulk properties of hexagonal PbI_2 crystal.

Molecular Weight	461.01 gm
Crystal Structure	Hexagonal
Lattice Constant	1.54 Å
Melting Point	402 °C
Boiling Point	954 °C
Density (Specific Gravity)	6.16 gm/ml

chemical reaction forms large sized particles and growth occurs by ripening. Nucleation and growth occur simultaneously in slow reactions. There is an inverse relationship between the rate of reaction and particle size where one increases and the other decreases, but the rate of reaction increases with an increase in the molarities of the reactant solution. When the absorption edge shifts to the higher energy, the particle size decreases and the quantum confinement effect is observed in semiconductor nanoparticles [47].

The role of thioglycerol acting as the capping agent in isolating the nanoparticles is extremely important. If a capping molecule binds in some way to a growing particle, it sticks there, arrests the growth and isolates it from the other growing particles in the reaction. Thus, an ideal capping molecule must reside on the surface of a particle. It forms a strong enough bond with the particle surface so that it remains there permanently, but should not take part in any other process occurring inside the particle. In other words, it should be able to avoid the coalescence of nanoparticles.

PbI_2 nanoparticles were stabilized using thioglycerol. By altering the concentration of the stabilizer, it was possible to populate the particles of certain sizes and energy gaps. The molarities of $Pb(NO_3)_2$ and KI were kept constant in the synthesis of PbI_2 nanoparticles (samples A and B). An accuracy of 10^{-5} gm and an accuracy up to 10^{-1} ml were maintained in the measurements of chemicals and solutions respectively [4-6]. PbI_2 is a hexagonal crystal with bulk properties as given in Table 1.

PbI_2 Thin Film Deposition

The PbI_2 thin film was deposited on the pre-cleaned FTO glass substrate by the CBD method using the precursor solution prepared by suspending the PbI_2 nanoparticle powder in double distilled water. The chemical bath deposited PbI_2 thin film (sample A) with approximately 12

μm thickness was created on the pre-cleaned FTO glass substrate. 2100 deposition times were required to prepare PbI_2 thin film (sample A). Similarly, PbI_2 thin film (sample B) approximately 27 μm in thickness was prepared with 4700 deposition times. The laser profilometer was used to measure the thicknesses of PbI_2 thin films. The structural, electrical, and optical properties of PbI_2 thin films (samples A and B) were improved by their heat treatment in air at 390°C for 30 minutes. The crystallinity of PbI_2 thin films increases and the resistivities, crystal defects and band gaps of thin films reduce by the heat treatment in air. There is an increase in the thickness of the film and the crystallite size and a decrease in the band gap and the thioglycerol concentration with an increase in the deposition time [4-6]. Mohammed et al. had similar observations [20].

RESULTS AND DISCUSSION

Ultraviolet-Visible Absorption Spectroscopy

This characterization technique was used to study the optical properties of PbI_2 nanoparticles [4-6]. The solubility of an ionic compound like PbI_2 increases by changing the solvent from acetonitrile to methanol, and the maximum solubility is provided by water. With acetonitrile as solvent, largest particles are obtained, as PbI_2 is least soluble in acetonitrile. When the solvent is methanol, the intermediate sized particles are formed, as PbI_2 is more soluble in methanol. As water is a better solvent for PbI_2 than methanol, smallest crystallites are obtained [9]. Acetonitrile is a better solvent for sample A having higher concentration of thioglycerol (0.8 M). Therefore, the largest-energy gap is obtained in the UV-Vis absorption spectrum of sample A which corresponds to the smallest colloidal crystallites. Sample B having low thioglycerol concentration (0.001 M) is least soluble in acetonitrile. Therefore, the large sized particles are obtained in sample B. Monodispersed particles were obtained in samples A and B. Lead iodide particles were dispersed in acetonitrile. Therefore, acetonitrile was used as the reference solution for PbI_2 nanoparticles.

The size dependence in semiconductor nanoparticles was determined from the UV-Vis absorption spectrum of the material [4-6]. UV-Vis absorption spectra were recorded at room temperature using Schimadzu UV-300 double beam spectrometer. The spectral range used in this case was 200 to 700 nm. The PbI_2 nanoparticle powders were dissolved in acetonitrile for UV absorption studies. It was confirmed that neither mercaptoethanol nor other chemicals used in the synthesis produce any absorption feature in this range.

Pb atoms arranged on hexagonal sheets are separated by iodine sheets by 7Å. PbI_2 is a IV-VII group layered semiconductor having alternate sheets of lead and iodine atoms. PbI_2 nanoparticles can be used for making the X-ray detectors. Their structures are anisotropic. The size confinement effects have been observed in the absorption and fluorescence spectra of the PbI_2 nanoparticles. This effect reflects the quantized motion of the small particles in a confined space which increases the effective band gap of the semiconductor. Other properties, and characteristics of these small colloidal particles, include enhanced redox activity and a tendency to grow in specific so-called magic numbers. There is a variation of 12 to 90 Å in the lateral dimensions of PbI_2 layered semiconductor. This variation depends on the nature of the growing cluster interface and also on the solvent [11]. The hexagonal symmetry determines the size of the PbI_2 cluster which increases by the symmetrical placement of lead atoms around a smaller cluster. The PbI_2 clusters having a single layer of ≈ 7Å thickness grow only to special sizes 12, 18 and 29 Å in the plane of the layer. The orientation of the PbI_2 crystallites (12, 18 and 29 Å) within the plane of the layer is similar to the symmetry of close-packed crystallites as that of bulk PbI_2 [9]. The existence of varying sizes of the PbI_2 crystallites can be understood by the hexagonal symmetry of PbI_2 clusters. The effective-mass approximation has been used to estimate the sizes of the PbI_2 anisotropic crystallites [1, 4, 48, 49].

The UV-Vis absorption spectra of PbI_2 nanoparticles (samples A and B) recorded from 200 to 700 nm at room temperature are shown in Fig. 2(a, b). The bulk band gap of lead iodide material is 2.57 eV at room temperature [9]. The UV-Vis absorption peak has appeared at 482 nm in the case of bulk lead iodide material

In PbI_2 nanoparticles (sample A), the UV-Vis absorption peaks have appeared at 360 nm (energy gap ~ 3.43 eV), 285 nm (energy gap ~ 4.35 eV) and 242 nm (energy gap ~ 5.14 eV) out of which the peaks at 285 nm and 360 nm are suppressed due to an increase in the molarity of thioglycerol (0.8 M) and the sharp excitonic peak has appeared

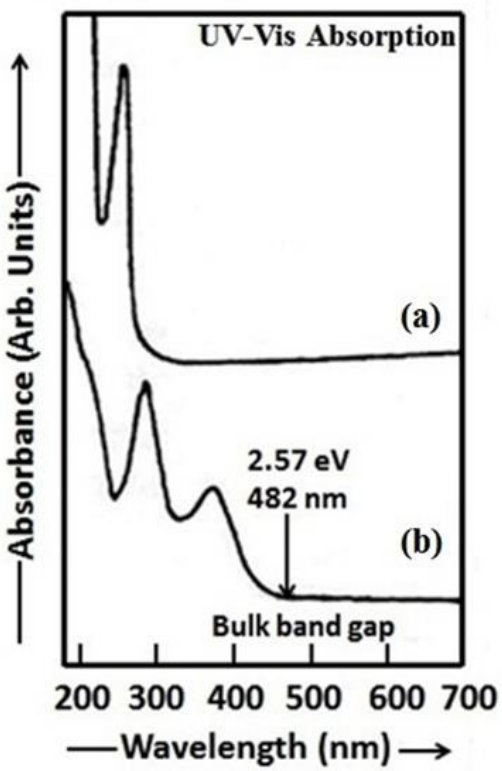

Fig. 2(a, b). UV-Visible absorption spectra of PbI_2 nanoparticles: a) sample A, and b) sample B.

at 242 nm. In PbI_2 nanoparticles (sample B), the UV absorption peaks have appeared at 360 nm (energy gap ~ 3.43 eV), 285 nm (energy gap ~ 4.35 eV), 242 nm (energy gap ~ 5.14 eV) and 215 nm (energy gap ~ 5.78 eV). An intense peak has appeared at 285 nm due to a decrease in the thioglycerol concentration. A change is observed in the colour of the materials due to the change in their absorption values. The colour of sample B is dark yellow while that of sample A is light yellow. In sample B, as the concentration of thioglycerol (0.001 M) is very less, the UV absorption peaks of samples A and B are obtained nearly at the same wavelengths but with different intensities. In sample A, the UV-Vis absorption peaks are blue shifted - 0.86 eV, 1.78 eV, 2.57 eV and in sample B, the peaks are blue shifted - 0.86 eV, 1.78 eV, 2.57 eV, 3.21 eV from the bulk PbI_2 band gap (2.57 eV). This indicates that there is an energy gap variation of 2.57 eV in sample A and that of 3.21 eV in sample B. From Fig. 2(a, b), it can be noticed that the sharpness of the excitonic peak reduces with a decrease in thioglycerol concentration. The effective mass approximation-based calculations [1, 4, 48, 49] were used to calculate the size of the PbI_2 particles. The equation of the exciton energy ΔE is given as

$$\Delta E = \frac{\hbar^2 \pi^2}{2R^2}\left[\frac{1}{m_e} + \frac{1}{m_h}\right] - \frac{1.8e^2}{\varepsilon R}. \quad (1)$$

The total size dependent energy gap is given as

$$E = E_g + \Delta E \quad (2)$$

Where E_g is the energy gap of the bulk semiconductor material and ΔE is the excited state energy. According to the effective mass approximation [1, 4, 48, 49], the sizes of the PbI_2 nanoparticles in samples A and B are estimated which are given in Table 2.

In samples A and B, it was possible to decrease the lead iodide particle size and correspondingly increase the energy gap by increasing the amount of thioglycerol. Change in the particle size can be correlated to the change in energy gap of the particles. According to Planck's quantum theory of radiation, the energy gap of the PbI_2 crystallites has been estimated using the equation of the energy of a photon $E = h\nu$ [4-6, 50]. As illustrated in Fig. 2(a, b) and Table 2, it was possible to adjust the thioglycerol concentration and the energy gap varied from 2.57 eV to 5.78 eV. As the energy

Table 2. Values of UV-Vis absorption wavelength, energy gap and particle size of PbI_2 nanoparticles (samples A and B).

Sample	Molarity of lead nitrate	Molarity of thioglycerol	Molarity of potassium iodide	Reference	UV-Vis absorption wavelength (nm)	Energy Gap (eV)	Particle Size (nm)
Sample A	0.01 M	0.8 M	0.05 M	Acetonitrile	360	3.43	6.05
					285	4.35	4.95
					242	5.14	4.39
Sample B	0.01 M	0.001 M	0.05 M	Acetonitrile	360	3.43	6.05
					285	4.35	4.95
					242	5.14	4.39
					215	5.78	4.06

gap for bulk PbI_2 crystal at room temperature is 2.57 eV, the energy gap variation of ~ 3.21 eV is achieved.

Thus, in our study, the PbI_2 nanoparticles were prepared in double distilled water at room temperature and the UV-Vis absorption spectra of these PbI_2 nanoparticles dispersed only in acetonitrile have been investigated. The particles having 3-4 sizes have been obtained in samples A and B, but the sharp excitonic peak is observed at smaller wavelength (242 nm) in sample A due to the higher thioglycerol concentration (0.8 M) and the intense peak is observed at higher wavelength (285 nm) in sample B due to the lower thioglycerol concentration (0.001 M). Thus, it is clear that the capping effect of thioglycerol is perfect in sample A and that it is not adequate in sample B.

The lateral dimensions of PbI_2 nanoclusters in samples A and B vary from 9 Å to 27 Å. The lateral dimension (L_{xy}) can be found out by using the band gap shift equation in anisotropic semiconductors [11] which is given by

$$\Delta E_g(eV) = \frac{\hbar^2}{2\mu_{xy}}\left[\frac{2\pi^2}{L_{xy}^2}\right] \frac{\hbar^2}{+2\mu_z}\left[\frac{\pi^2}{L_z^2}\right] \quad (3)$$

Where μ_{xy} is the reduced effective mass of electron-hole pairs within the layer planes and μ_z is the reduced effective mass of electron-hole pairs perpendicular to the layer planes. L_{xy} and L_z are the corresponding lateral dimensions of the clusters in angstroms. The first and second terms on the right side of equation 3 are the ground state energies of electrons and holes within the layer planes and perpendicular to the layer planes respectively. The value of μ_{xy} is 0.32 electron mass and that of μ_z is 1.4 electron mass for PbI_2 nanoclusters. The thickness of a single PbI_2 layer is L_z = 7 Å [11]. The equation 4 becomes

$$\Delta E_g(eV) = \frac{235}{L_{xy}^2} + 0.55. \quad (4)$$

Considering the planer growth of sandwiched layers, it has been concluded that the growth is laminar with three particle sizes viz 12 Å, 16 Å and 24 Å consistent with UV-Vis absorption results. These dimensions of PbI_2 nanoclusters prepared in acetonitrile have been reported which are 12Å, 16 Å and 24 Å. The PbI_2 clusters having 12 Å diameter were analysed by TEM [11]. The PbI_2 cluster with lateral dimension of ~ 12 Å grows from a seed nucleus which contains the closed packed hexagonal array of iodine atoms. The next PbI_2 cluster with lateral dimension of ~ 16 Å grows from the 12 Å nucleus. This process is repeated producing a 24 Å crystallite [11]. The hexagonal symmetry is shown by the PbI_2 cluster in the metal plane. The 16 Å is a special, magic size of the PbI_2 cluster in which the hexagonal arrays of metal atoms appeared on the edges of the micro crystallites. This is because the PbI_2 cluster size of 16 Å is common in both PbI_2 and BiI_3 systems which grows from the 12 Å nucleus. At 16 Å size, a slight difference was observed in the structure of PbI_2 and BiI_3. PbI_2 showed the hexagonal symmetry while BiI_3 showed the honeycombed symmetry in the metal plane. 16 Å is the largest size of both the PbI_2 and BiI_3 clusters which have similar interfacial energies. The hexagonal and honeycombed symmetries of PbI_2 and BiI_3 clusters grow from the lateral dimension of 16 Å and the microcrystalline interfaces are obtained with different structures and reactivities [11]. This is shown in the structure of PbI_2 and BiI_3 clusters having the lateral dimensions greater than 16 Å (Fig. 3).

The lateral dimensions of PbI_2 nanoparticles in samples A and B are comparable to that of lead iodide particles prepared by Sandroff group [11]. The standard and observed values of L_{xy} are given in Table 3.

Fig. 4 shows the variation of quantization energy or band gap shift ΔE_g (eV) with lateral

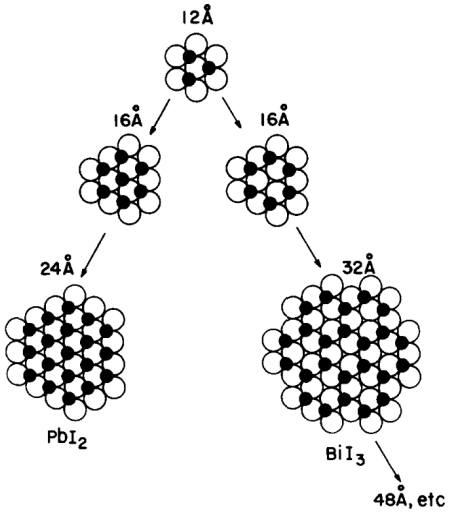

Fig. 3. The hexagonal structure of PbI_2 clusters and the honey-combed structure of BiI_3 clusters [11].

dimension L_{xy} (Å). The values of the energy gap of PbI_2 nanoparticles prepared by Sheng *et al.* [13] are lower than those of PbI_2 nanoparticles obtained in our study. Thus, the absorption wavelengths observed in the UV-Vis absorption spectra of PbI_2 nanoparticles synthesized in our study are lower than those of PbI_2 nanoparticles prepared by Sheng *et al.* [13].

Sandroff *et al.* [11] prepared the PbI_2 clusters in colloidal form at room temperature in the absence of stabilizing agent using the aqueous chemical method. Sandroff *et al.* [11] observed the UV-Vis absorption spectra of colloidal PbI_2 prepared in a variety of polar solvents. Significant variations are seen in the relative intensities of absorption peaks as well as the commencement of absorption when the solvent is changed from acetonitrile to methanol to water. PbI_2 in acetonitrile exhibits prominent excitonic peaks, which become less sharp at the smallest particles size. As water is a better solvent for PbI_2 than methanol, smallest crystallites are formed in water, whereas, PbI_2 being least soluble in acetonitrile, largest particles are created [11]. We obtained the PbI_2 nanoparticles at room temperature in the presence of the capping agent using the aqueous chemical method. Since acetonitrile is a better solvent, we were able to achieve the smallest particles in samples A and B when we recorded the optical absorption spectra of PbI_2 nanoparticles.

Sengupta *et al.* [51] prepared the PbI_2 nanoparticles at room temperature in the absence of surfactants using the method followed by Sandroff *et al.* [9]. From the UV-Vis absorption spectra of PbI_2 nanoparticles recorded by Sengupta *et al.* [51], it can be seen that the optical absorption bands are observed at the peaks similar to those observed in our samples. The quantum confinement effect can be observed due to a decrease in the average particle size caused by photodecomposition of larger particles [49, 52]. The particle size decreases by aging under light.

X-ray Diffraction

The XRD analysis of dry PbI_2 nanoparticle powders has been done using a Philips PW 1840 powder X-ray diffractometer. CuKα (λ = 1.542 Å) has been used as the source of incident radiation. The spectral range 5° to 80°was used to record the XRD patterns of PbI_2 nanoparticles [4-6]. The structural properties of the PbI_2 nanoparticles (samples A and B) have been studied by using the XRD patterns. The XRD diffraction has been used to determine the phase of the nanoparticles and also their size measurements. When the observed and standard values of PbI_2 (standard ASTM) data are compared, they match with each other. The hexagonal structure was observed in PbI_2 nanoparticles. The XRD patterns of PbI_2 nanoparticles (samples A and B) having various molarities of thioglycerol are shown in Fig. 5(a, b). The Debye-Scherrer formula was used to estimate the average size of the PbI_2 nanoparticles, $d_{XRD} = \frac{0.9\lambda}{\beta \cos\theta}$ [4, 6, 24, 43, 53]. In sample A, the XRD peaks are not visible, the size of the PbI_2 particles cannot be found out because

Table 3. Standard and observed values of lateral dimension (L_{xy}), energy gap (E_g) and band gap shift (ΔE_g).

Observed Values				Standard Values [10]			
UV Absorption (λ) nm	Energy Gap (E_g) eV	Band Gap Shift (ΔE_g) eV	Lateral dimension of Cluster (L_{xy}) Å	UV Absorption (λ) nm	Energy Gap (E_g) eV	Band Gap Shift (ΔE_g) eV	Lateral dimension of Cluster (L_{xy}) Å
360	3.43	0.86	27.53	363	3.42	0.85	27.98
285	4.35	1.78	13.04	314	3.95	1.38	16.82
242	5.14	5.14	10.78	258	4.8	2.23	11.82
215	5.78	5.78	9.39				

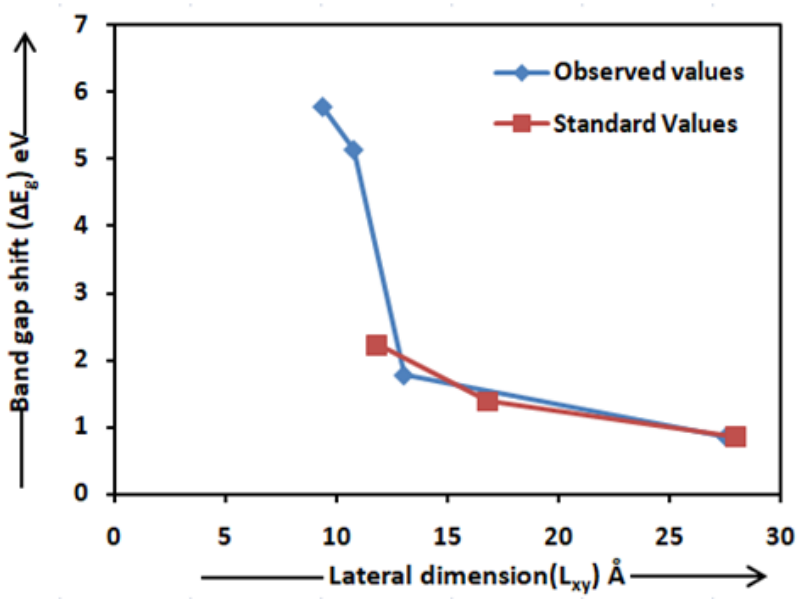

Fig. 4. Variation of quantization energy or band gap shift ΔE_g (eV) with lateral dimension L_{xy} (Å) in PbI_2 nanoparticles.

very small sized particles were obtained due to higher concentration of thioglycerol (0.8 M). In sample B, the calculated value of the interplanar spacing 'd' by using the Bragg's condition is 3.435 A°. The cluster size 'd_{XRD}' is 20.39 nm. The size of the cluster 'd' is found out by using the Debye-Scherrer formula. The XRD peaks of small widths are observed in sample B. The large sized PbI_2 particles were obtained in sample B due to lower concentration of thioglycerol (0.001 M). Additional evidence for the capping effect is provided by the XRD data, which show that it is perfect at higher thioglycerol concentrations and imperfect at lower concentrations. The value of δ of PbI_2 nanoparticles in sample B is 2.405×10^{15} lines/m^2 which was calculated by using the formula of dislocation density (δ), $\delta = \frac{1}{d_{XRD}^2}$[9, 10, 41]. The first peak, second peak, third peak, ...eighteenth peak correspond to the reflection of crystal planes (001), (101), (102), (003), (110), (111), (103), (210), (004), (200), (113), (104), (203), (211), (114), (212), (105), (300) respectively. The intensity of peaks for these planes is found to be noticeably enhanced in sample B. The maximum intensity of the diffraction peak which was observed along (101) and (102) planes indicate the growth of PbI_2 nanoparticles along these two planes.

The hexagonal structure is suggested by the diffraction peaks at their (102), (101), as well as other planes. The investigation of the powder X-ray diffraction by Debye function analysis [54] confirms that the PbI_2 particles having a hexagonal structure are polycrystalline in nature. Similar observations were found in the case of PbI_2 thin films prepared by Mohammed *et al.* [24]. The average crystallite size d_{XRD} of PbI_2 nanoparticles

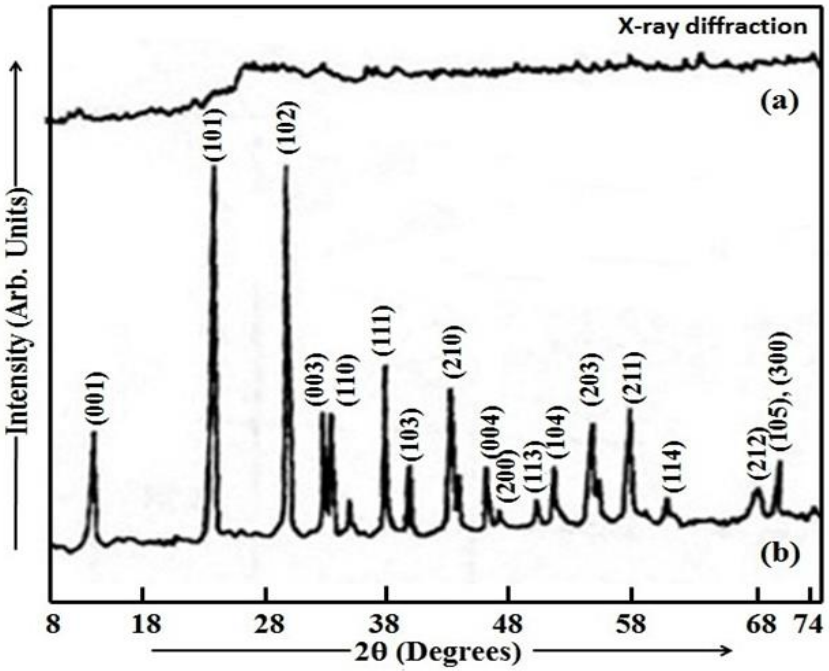

Fig. 5(a, b). X-ray diffraction patterns of PbI_2 nanoparticles: a) sample A, and b) sample B.

prepared in our study is smaller than that of PbI_2 nanoparticles deposited on glass substrate by Mohammed *et al.* using the thermal evaporation method [24].

Dag *et al.* [10] have synthesized PbI_2 nanocrystals by the method utilised by Sandroff *et al.* [11]. In these cases, the nanocrystals were grown in colloidal solutions, in zeolite cages, or in copolymer films. Dag *et al.* [10] described the study of PbI_2 nanocrystals embedded in silica glass, prepared by the sol-gel technique. This technique enables the growth of stable nanocrystals with a controlled size, within the solid and transparent medium. The layered structure consisting of corresponding bulk PbI_2 crystallites possesses a strong intra-layer bonding yet only weak, so called van der Walls inter-layer interactions. This layered structure creates a strong anisotropy in the physical and electronic properties. The bulk layers can be stacked in a variety of ways to form different polytypes. In this work, the investigation of PbI_2 nanocrystals shows that these nanocrystals have a 2H polytype with a D_{3d} space group, confirmed by the XRD measurements.

X-ray Photoelectron Spectroscopy

In order to check the presence of impurity, XPS analysis of dry PbI_2 powders was performed using a commercial model ESCALAB MK II of VG Scientific, U.K. MgKα (hυ = 1253.6 eV) has served as the source of radiation and photoelectrons were analyzed using a concentric hemispherical analyzer at a 50 eV pass energy.

Table 4 shows the elements present, their atomic concentration, binding energies and concentration ratios of different elements. The presence of carbon and oxygen elements has been observed in PbI_2 nanoparticles (samples A and B) because of the organic capping agent like thioglycerol. The Pb $4f_{7/2}$ core level appears at the binding energy (138.5 eV) which corresponds to PbI_2 (sample A) and the Pb $4f_{7/2}$ core level appears at the binding energy (138 eV) which corresponds to PbI_2 (sample B). The I $3d_{5/2}$ core level appears at the binding energy (617.7 eV) which corresponds to PbI_2 (sample A) and the I $3d_{5/2}$ core level appears at the binding energy (617 eV) which corresponds to PbI_2 (sample B). The results of XPS characterization have not been reported in the previous literature.

Fig. 6(a, b) shows the XPS scans of Pb (Lead) element in PbI_2 nanoparticles (samples A and B). Fig. 7(a, b) shows the XPS scans of I (Iodine) element in PbI_2 nanoparticles (samples A and B) and Fig. 8(a, b) shows the XPS survey scans of PbI_2 nanoparticles (samples A and B).

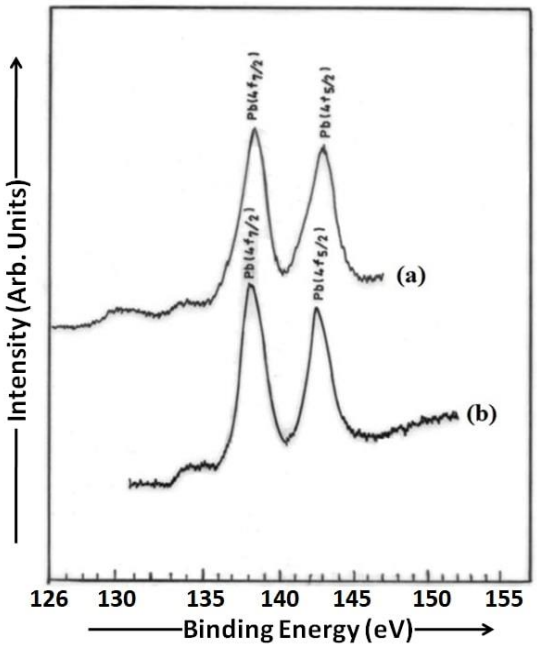

Fig. 6(a, b). XPS scans of Pb (Lead) element in PbI_2 nanoparticles: a) sample A, and b) sample B.

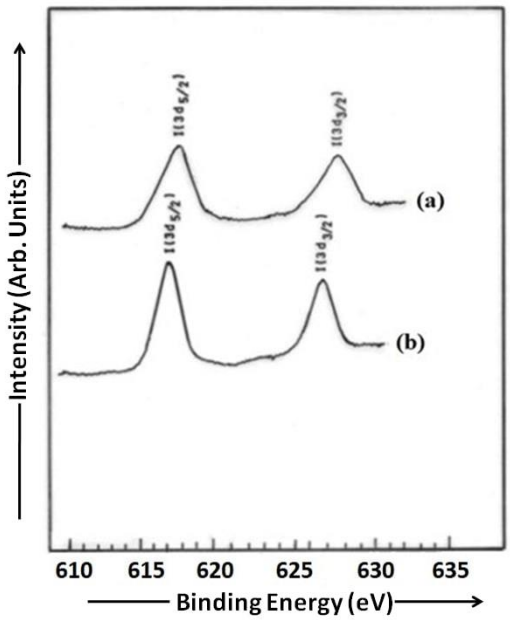

Fig. 7(a, b). XPS scans of I (Iodine) element in PbI_2 nanoparticles: a) sample A, and b) sample B.

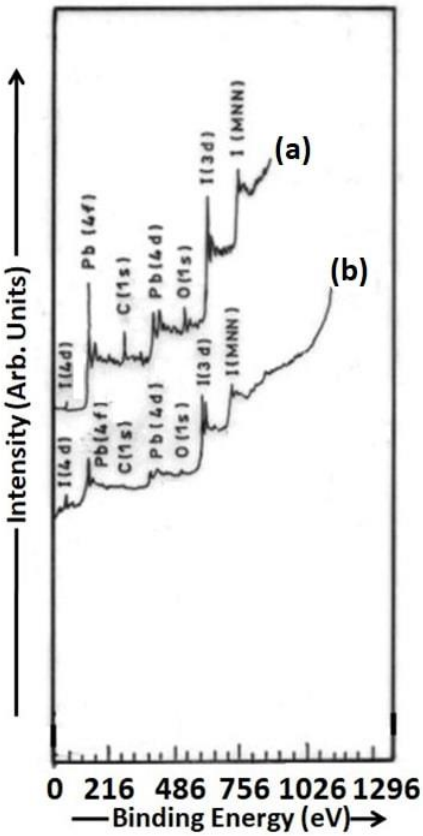

Fig. 8(a, b). XPS survey scans of PbI_2 nanoparticles: a) sample A, and b) sample B.

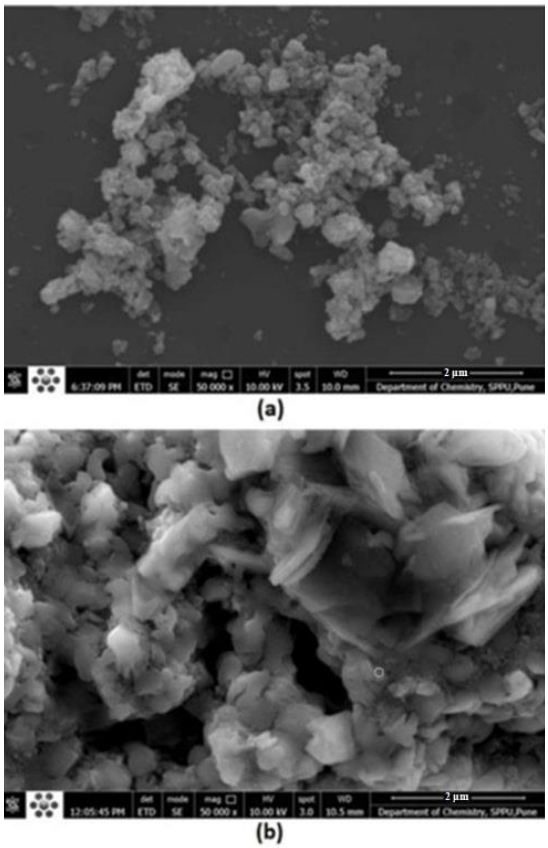

Fig. 9(a, b). SEM images of PbI_2 thin films: a) sample A, and b) sample B; with magnification of 50,000 in both the samples. Scale bar: 2 µm.

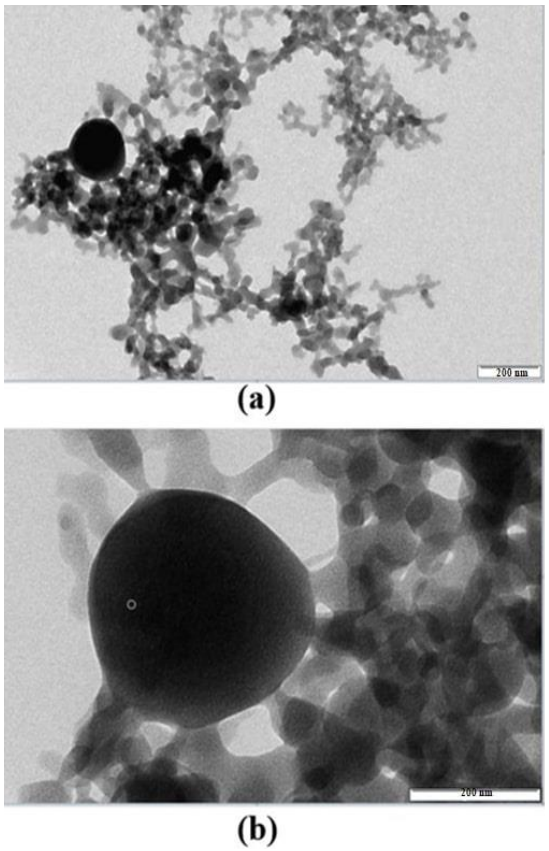

Fig. 10(a, b). TEM images of PbI_2 nanoparticles: a) sample A, and b) sample B; with magnification of 200 nm in both samples.

Surface Morphological Analysis

Scanning Electron Microscopy

The SEM images of CBD deposited PbI_2 thin films (samples A and B) with uniform distribution of PbI_2 nanoparticles are shown in Fig. 9(a, b). The aggregation of particles has been observed in both the samples. The enhancement in deposition time decreases the film uniformity and increases the number of material grains [4-6]. The morphology and structure of PbI_2 nanoparticles are presented by the SEM micrographs of samples A and B. In sample A, the cylindrical PbI_2 clusters are produced and in sample B, the platelets like PbI_2 grains are obtained. Thioglycerol controls the growth of lead iodide nanoparticles.

Lifshitz *et al.* [55] recorded a typical SEM micrograph of the Q-size PbI_2 particles embedded in SiO_2 films. These particles were prepared by a sol-gel technique. The size distribution of these particles was determined using a scanning electron microscope. Lifshitz *et al.* [55] observed a rugged structure with cracks 5-10 µm in width. As the deposited films exhibit a flat surface, most of the physical measurements were performed on the deposited films [55]. We recorded the SEM micrographs of samples A and B (CBD deposited PbI_2 thin films) prepared without using silica. A scanning electron microscope determines the size distribution of these nanoparticles.

Transmission Electron Microscopy

The TEM micrographs of PbI_2 nanoparticles (samples A and B) are shown in Fig. 10(a, b). The size of the PbI_2 nanoparticles i.e. sample B which were dissolved in acetonitrile was measured by TEM. In sample B, approximately 20 to 30 nm sized PbI_2 particles are obtained as the concentration of thioglycerol is very less which is 0.001 M. The sample B is least soluble in acetonitrile. The large sized spherical PbI_2 grains are observed in sample B. As acetonitrile is a better solvent for sample A, the small sized spherical PbI_2 clusters are obtained in sample A.

Sandroff *et al.* [11] recorded the transmission

electron micrographs of PbI_2 clusters. TEM was used to determine the sizes of these clusters. The PbI_2 clusters were circular in shape with the largest cluster displaying hexagonal facets. Sandroff *et al.* [11] was not able to measure the size of the particles smaller than ~ 1.6 nm in acetonitrile colloids. The sizes of these particles were confirmed by TEM for aqueous colloids of PbI_2. As the particle density on the grid was quite uniform and low in acetonitrile, it is difficult to confidently distinguish the particles smaller than ~ 1.2 nm from the grainy structure of the supporting film. In case of water, it was possible to measure the size of the particles less than or greater than 1.2 nm [11]. In our case, the size of the PbI_2 particles in sample B is ~ 20 to 30 nm. The large sized particles are obtained due to lower concentration of thioglycerol. Thus, it was possible for us to measure the size of these particles in acetonitrile colloids by TEM. Only in case of sample B, we could not measure the size of the particles by TEM for aqueous colloids of PbI_2.

Lifshitz *et al.* [55] recorded the TEM micrographs of PbI_2 nanocrystals embedded in SiO_2 films. PbI_2 nanocrystals having mean particle diameter ranging from 5 nm to 20 nm have been prepared. The TEM micrographs could not determine the mean particle diameter of specimens whose particles are smaller than 8 nm. This is because small particles are unstable under the high-energy electron beam. The nanocrystals prepared by Lifshitz *et al.* [55] exhibited polyhedron morphology. We recorded the TEM micrograph of PbI_2 nanoparticles (sample B) with diameter ranging from 20 to 30 nm. Therefore, the size of such larger particles can be found out accurately from the TEM micrograph as the large particles are stable under the high energy electron beam.

Atomic Force Microscopy

The AFM characterization was used to investigate the surface morphology of CBD deposited PbI_2 thin films (sample A and sample B). The 2D-AFM images (a) and the 3D-AFM images (b) of sample A and sample B deposited at different times are illustrated in Fig. 11(a, b) and Fig. 12(a, b) respectively. The

material clusters consisting of nanoparticles of various sizes are demonstrated by the surface topology [4]. The average size of the PbI_2 grains observed in sample A varies from 21.15 nm to 75.03 nm and the average size of the PbI_2 grains observed in sample B varies from 48.73 nm to 168.3 nm with different magnifications [4, 5, 6]. The size of the PbI_2 grains present in sample A shown in Fig. 11(a, b) is 33.55 nm and that in sample B shown in Fig. 12(a, b) is 83.06 nm. With increasing deposition time, the particle size increases and the film uniformity decreases [5, 6]. The 2D-AFM images (a) show the presence of the highly dense cylindrical PbI_2 grains in samples A and B. The 3D-AFM images (b) show the presence of the hills and valleys in samples A and B. The size and height of the PbI_2 grains are dependent on the discontinuity observed in the 2D-AFM and 3D-AFM images of samples A and B. The height of the hills observed in the 3D-AFM image of sample B is higher than that observed in the 3D-AFM image of sample A due to the variation in the PbI_2 film thickness with the deposition time [5, 6].

Liu *et al.* [14], have synthesized and optically characterized 2D few-layer PbI_2 flakes at both room and cryogenic temperatures. On a plasma treated Si/SiO_2 substrate, they had dropped a solution of saturated PbI_2 powder, followed by heating to 180°C within 5 minutes for the nucleation of PbI_2 flakes and nanoparticles in ambient environment. In the SEM image their PbI_2 particles were hexagonal or triangular in shape, while their thicknesses were between several to hundreds of nanometers as evident from AFM [14]. We recorded the AFM images of samples A and B (CBD deposited PbI_2 thin films) prepared without using silica.

Elemental composition analysis

Energy-dispersive X-ray spectroscopy (EDX)

The EDX spectrum of CBD deposited PbI_2 thin film (sample A) is shown in Fig. 13 and that of CBD deposited PbI_2 thin film (sample B) is shown in Fig. 14. The composition of the elements present in PbI_2 nanoparticles was given in stoichiometeric atomic percentages by EDX method [4-6]. The large depth profile in EDX was ≈ 1 micron. Due to this substantial depth profiling, it was easy to detect the elements like lead, iodine, sulphur, carbon, oxygen and potassium present in samples A and B in stoichiometric atomic percentages.

From Table 4, Table 5, and Table 6, we can observe the difference in the atomic concentration of the elements. The reason for this difference may be the large depth profile in EDX which is ≈ 1 micron. This extensive depth profiling is not possible in XPS. In XPS, one can get the information only from the surface. The detection of Sulphur

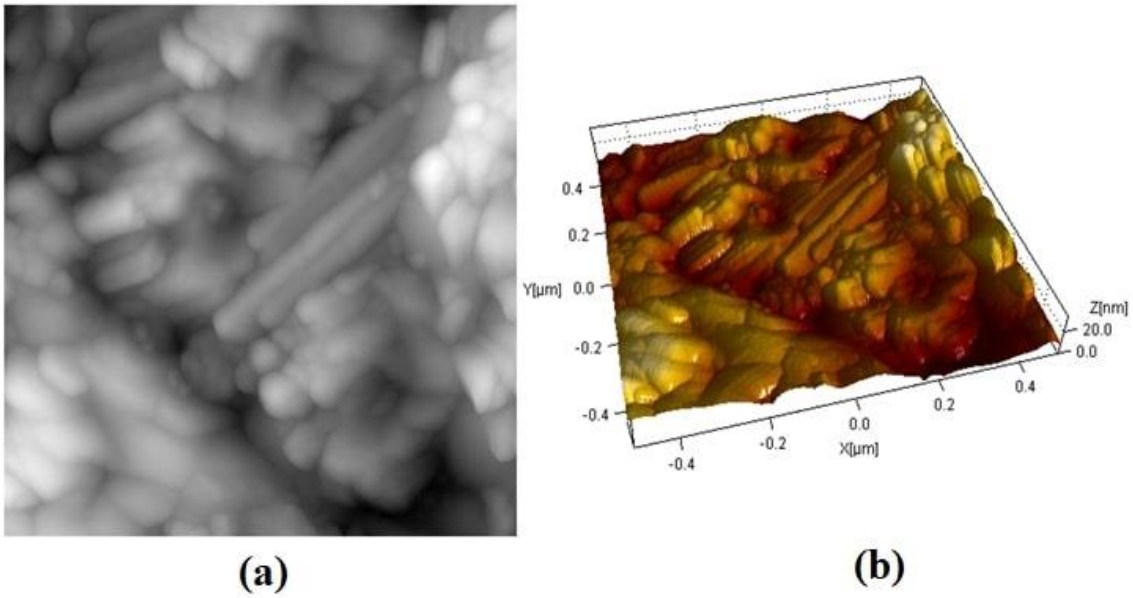

Fig. 11(a, b). 2D-AFM image (a) and 3D-AFM image, (b) of PbI_2 thin film (sample A).

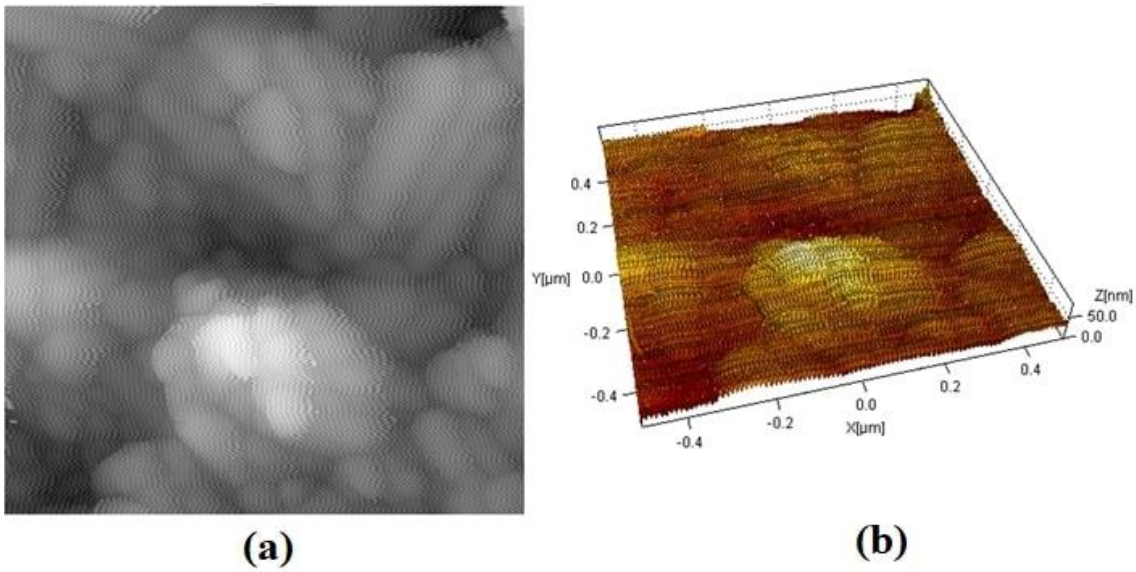

Fig. 12(a, b). 2D-AFM image (a) and 3D-AFM image, (b) of PbI_2 thin film (sample B).

element in samples A and B is possible in EDX analysis, but it is not possible in XPS analysis. This can be explained by the same reason as above.

The presence of the elements like carbon (C), oxygen (O), sulphur (S), lead (Pb), potassium (K) and iodine (I) in atomic percentages in PbI_2 thin film (sample A) is shown in Table 5 and that in PbI_2 thin film (sample B) is shown in Table 6.

The value of Pb:I ratio for both the samples A and B is 0.49. From this value of lead to iodine ratio, it can be clearly seen that the stoichiometry of PbI_2 thin films (samples A and B) is nearly perfect.

Similar studies have been published like TOF-ERDA (Time-of-flight-elastic recoil detection analysis) [15], AAS (Atomic Absorption Spectroscopy) [56], TGA (Thermogravimeteric Analysis), LEIS (Low-Energy Ion Scattering) etc. which can also indicate the presence of the sulphur element in PbI_2 thin films due to their thioglycerol capping [57].

It was not possible by the EDX analysis to detect the presence of the hydrogen element (H)

Table 4. X-ray Photoelectron Spectroscopy Data of PbI_2 Nanoparticles (Samples A and B).

PbI_2	Elements	B.E.	Area (mm^2)		Area (cm^2)	Sensitivity Factor (SF)	Area/SF	ΣArea/SF	Ratio of elements	Concentration of elements %
			10K	3K						
PbI_2 (Sample A) TG = 0.8 M	C(1S)	285.5	864	2880	8.64	0.205	42.14	68.31	Pb:I = 1.172	61.69
	O(1S)	532.8	532.8	1776	5.328	0.63	8.457		Pb:O = 1.13	12.37
	Pb(4f)	138.5	2440	8133.3	24.40	2.55	9.568			13.99
	I(3d)	617.7	3588	11960	35.88	4.4	8.154			11.93
PbI_2 (Sample B) TG = 0.001 M	C(1S)	285	213	710	2.13	0.205	10.39	33.98	Pb:I = 0.695	30.57
	O(1S)	533.6	230	766.6	2.30	0.63	3.65		Pb:O = 2.241	10.74
	Pb(4f)	138	2086	6953.3	20.86	2.55	8.18			24.07
	I(3d)	617	5175	17250	51.75	4.4	11.76			34.60

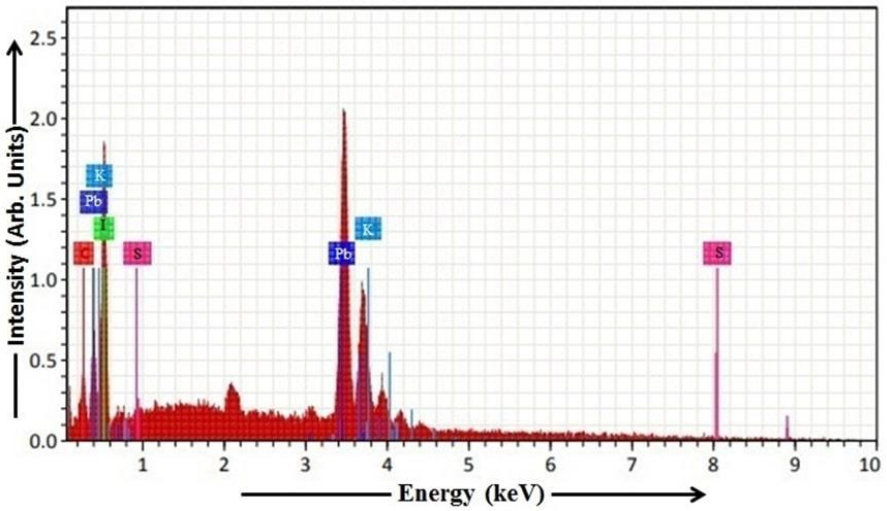

Fig. 13. EDX spectrum of PbI_2 thin film (sample A).

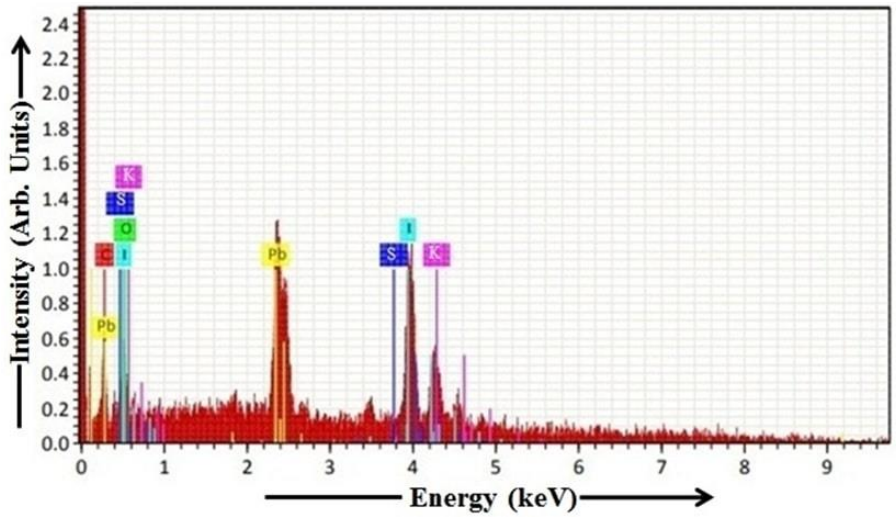

Fig. 14. EDX spectrum of PbI_2 thin film (sample B).

in PbI_2 thin films deposited on silicon (Si) and FTO glass substrates using the ALD method by Popov et al. [15]. The EDX study was capable of detecting the carbon (C) and nitrogen (N) elements but these elements could not be evaluated accurately. Only the tin (Sn) and silicon (Si) elements could be evaluated by the EDX analysis [15]. In our study, the carbon (C), oxygen (O), sulphur (S), lead (Pb), potassium (K) and iodine (I) elements could be detected and also evaluated accurately by the EDX study.

Photoluminescence Analysis

The photoluminescence emission spectra recorded for PbI_2 nanoparticles (samples A and B) at room temperature are shown in Fig. 15(a, b).

The excitation wavelength range of 292 to 317 nm and the emission wavelength range of 317 to 700 nm were used to record the PL spectra of PbI_2 nanoparticles (sample A) at room temperature. In sample A, the PbI_2 particles were excited at 302 nm and three emission peaks at about 331 nm (energy gap ~ 3.75 eV), 416 nm (energy gap ~ 2.98 eV) and 528 nm (energy gap ~ 2.35 eV) were observed. The photoluminescence intensity of the peak observed at 416 nm is maximum. The excitation wavelength range 291 to 316 nm and the emission wavelength range 316 to 700 nm were used to record the PL spectra of PbI_2 nanoparticles (sample B) at room temperature.

Table 5. EDX data of PbI_2 thin film (sample A).

Element	At. No.	Netto	Mass [%]	Mass Norm [%]	Atom [%]	abs. error [%] (1 sigma)	rel. error [%] (1 sigma)
Carbon	6	625	1.27	1.29	30.87	0.36	27.96
Oxygen	8	2687	6.98	7.10	12.49	0.31	4.43
Sulphur	16	0	0.00	0.00	0.00	0.00	10.00
Lead	82	21390	61.95	63.00	17.13	2.14	3.45
Potassium	19	3111	11.22	11.41	4.80	0.47	4.23
Iodine	53	6473	16.91	17.20	34.71	2.56	15.12
			Sum:	98.33 100.00	100.00		

Table 6. EDX data of PbI_2 thin film (sample B).

Element	At. No.	Netto	Mass [%]	Mass Norm [%]	Atom [%]	abs. error [%] (1 sigma)	rel. error [%] (1 sigma)
Lead	82	3792	31.37	32.06	20.16	1.32	4.21
Sulphur	16	635	7.60	7.77	1.28	0.46	6.10
Oxygen	8	309	1.50	1.54	9.92	0.52	34.42
Carbon	6	450	2.57	2.63	25.57	0.77	29.84
Iodine	53	3663	46.74	47.76	40.95	1.87	4.00
Potassium	19	522	8.07	8.25	2.12	0.53	6.55
			Sum:	97.85 100.00	100.00		

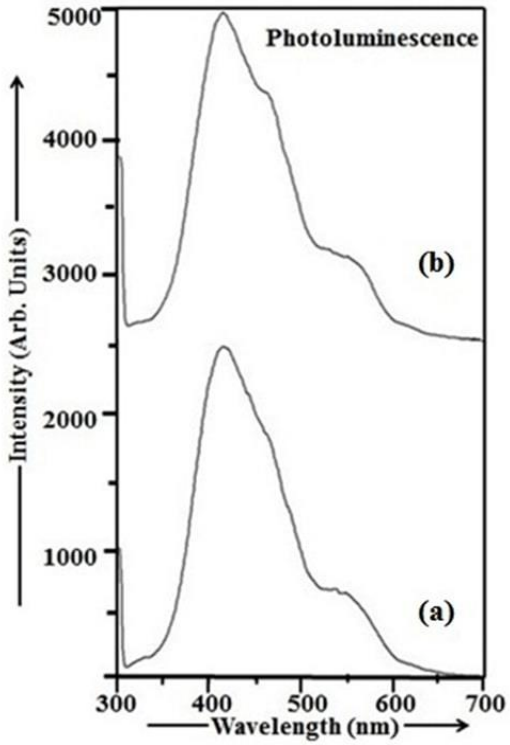

Fig. 15(a, b). Photoluminescence spectra of PbI_2 nanoparticles: a) sample A, and b) sample B.

In sample B, the PbI_2 particles were excited at 301 nm and three emission peaks at about 329 nm (energy gap ~ 3.77 eV), 414 nm (energy gap ~ 3.00 eV) and 526 nm (energy gap ~ 2.36 eV) were observed. The photoluminescence intensity of the peak observed at 414 nm is maximum. The luminescence peaks were observed at smaller wavelengths in the PL spectrum of sample B as compared to the emission peaks observed in the PL spectrum of sample A [4, 5, 6].

The shift was observed in the emission wavelengths at smaller values in the PL spectra of PbI_2 nanoparticles synthesized by using the aqueous chemical method in our study as compared to the PL spectra of PbI_2 films prepared by Sheng *et al.* [13].

The shift was observed at higher emission wavelengths in the PL spectra of PbI_2 nanoparticles embedded in porous silica films [10] in comparison with the PL spectra of PbI_2 nanoparticles obtained in the present study. The shift was also observed at higher luminescence wavelengths in the PL spectra of 2D few-layer PbI_2 flakes prepared by Liu *et al.* [14] as compared to the PL spectra of PbI_2 nanoparticles prepared in this study.

The shift was observed at higher emission wavelengths in the PL spectra of PbI_2 nanoparticles embedded in porous silica films [10] in comparison with the PL spectra of PbI_2 nanoparticles obtained in the present study. The shift was also observed at higher luminescence wavelengths in the PL spectra of 2D few-layer PbI_2 flakes prepared by Liu *et al.* [14] as compared to the PL spectra of PbI_2 nanoparticles prepared in this study.

The continuous wave PL (CW-PL) spectra were recorded at various temperatures and with various excitation powers by Dag et al. [10]. The PL spectra of specimens with mean particle radii of 4.7 and 6.0 nm were recorded at 77 K with an excitation intensity of 1.4 W/cm^2 by Dag *et al.* [10]. Qualitatively, the spectra are similar, consisting of three bands, a sharp exciton peak and two deeper L and G bands. However, they differ in a number of ways from one another. The exciton energy in the sample with diameter of 4.7 nm is blue shifted in comparison with the 6.0 nm sized specimen. Thus, it is clear that the quantum size effect is observed. In addition, the 6.0 nm sized specimen's L band is dominant, while its G band is weak. In the 4.7 nm sized specimen, the integrated intensity of the G band is larger than the integrated intensity of its L band [10]. In our case, the blue shift was observed in the luminescence wavelengths in the PL spectra of PbI_2 nanoparticles (samples A and B).

Due to a drastic change in the physical properties of PbI_2 nanoparticles as compared to the bulk PbI_2 material shown by the characterization results, these nanoparticles are used in various industrial applications. Attempts were made to determine the potential of PbI_2 nanoparticles in applied area. After a detailed discussion, we discovered that the layered PbI_2 semiconductor nanoparticles and also PbI_2 thin films are widely used in optoelectronic and photovoltaic device applications, radiation detection and several other applications [12, 15, 22]. Electroluminescent devices, single electron transistors etc. have been devised which enabled us to obtain compact, energy saving, high efficiency devices using PbI_2 nanoparticles in the present study [12].

The experimental part of the preparation of PbI_2 nanoparticles was carried out in the absence of nitrogen atmosphere. The oxidation of PbI_2 nanoparticles could be prevented in the presence of nitrogen atmosphere due to which the sharp excitonic absorption peaks and the broad XRD peaks would have appeared in the UV-Vis absorption spectra and the XRD spectra of samples A and B respectively. In our previous work, the cadmium sulphide (CdS) nanoparticles, the copper sulphide (Cu_2S), nanoparticles and the manganese doped cadmium sulphide (CdS:Mn) nanoparticles were synthesized under nitrogen atmosphere to avoid the oxidation of nanoparticles [4-7]. However, it may be worthwhile to investigate the effect of temperature on the synthesis.

CONCLUSION

It was possible to synthesize the PbI_2 layered semiconductor nanoparticles by using the organic capping agent like thioglycerol in aqueous medium. The small sized, monodispersed PbI_2 particles were obtained by increasing the concentration of stabilizer. Particles exhibited absorption peaks at 360 nm, 285 nm, 242 nm and 215 nm indicating the occurrence of magic numbers. The band gap of PbI_2 semiconductor is 2.57 eV at room temperature. The energy gap variation between 2.57 eV to 5.78 eV was observed in PbI_2 nanoparticles. The XRD analysis showed the hexagonal structure of PbI_2 nanoparticles.

The quantum size effect was observed in undoped PbI_2 nanoparticles. The shift was observed at smaller absorption wavelengths in

the UV-Vis absorption spectra and at smaller luminescence wavelengths in the PL spectra of PbI_2 nanoparticles. TEM analysis showed that approximately 20-30 nm sized, circular PbI_2 particles were obtained in sample B, as these PbI_2 particles are least soluble in acetonitrile. As the PbI_2 particles in sample A are more soluble in acetonitrile, a smaller sized spherical PbI_2 particles were produced in sample A.

The CBD deposited PbI_2 thin films were investigated by SEM and EDX. The shape and size distribution of the lead iodide particles were determined using the scanning electron microscopy. The small sized PbI_2 particles have cylindrical form and the large sized particles (~ 20 nm diameter) have platelet form. The PbI_2 particles are of hexagonal phase. The atomic percentage ratio of lead and iodine elements present in PbI_2 thin films (samples A and B) was 0.49. Both PbI_2 samples had nearly perfect stoichiometry. The highly dense cylindrical PbI_2 grains are observed in the 2D-AFM images and the hills and valleys are visible in the 3D-AFM images of PbI_2 thin films. The PbI_2 thin films have large commercial applications like optoelectronic and solar cell applications.

ABBREVIATIONS

PbI_2 - Lead Iodide
FTO - Fluorine doped Tin Oxide
CBD - Chemical Bath Deposition
UV-Vis - Ultraviolet-Visible
XRD - X-ray diffraction
XPS – X-ray Photoelectron Spectroscopy
PL - Photoluminescence
TEM - Transmission Electron Microscopy
SEM - Scanning Electron Microscopy
EDX – Energy-Dispersive X-ray Spectroscopy
AFM – Atomic Force Microscopy

ACKNOWLEDGEMENT

We thank the SEM, EDX, Mapping and XRD operators of Chemistry Department of Savitribai Phule Pune University for performing the SEM, EDX, Mapping and XRD measurements, the Head of Chemistry Department of Savitribai Phule Pune University for providing the UV-Vis Absorption and PL instruments access. Also, we thank the XPS and AFM operators of Physics Department of Savitribai Phule Pune University, the TEM operator and the operator of thin film thickness measurement of IIT Powai, Mumbai for doing the TEM and thin film thickness measurement characterizations respectively.

CONFLICT OF INTEREST

The authors declared no competing financial interest.

Author Contribution

Darekar M. S. was the main author, conducted the experimental work: Dip coating deposition of Cu_2S nanoparticles, material investigation, thin film characterization, device fabrication assessment and development and completed the paper: interpretation of results, understanding the science behind materials and devices, drafting of manuscript, drawing diagrams and tables and plotting graphs. Praveen B.M. supervised the manuscript preparation process.

Source of funding: The author(s) received no financial support for this research.

REFERENCES

[1] Brus L. E., (1986), Electronic wave functions in semiconductor clusters: Experiment and theory. J. Phys. Chem. 90: 2555-2560. https://doi.org/10.1021/j100403a003

[2] Henglein A., (1987), Mechanism of reactions on colloidal microelectrodes and size quantization effects electrochemistry II. Topics in Current Chem.143: 113-180. https://doi.org/10.1515/9783112539248-008

[3] Alivisatos A. P., (1996), Semiconductor clusters, nanocrystals and quantum dots. Science. 271: 933-937. https://doi.org/10.1126/science.271.5251.933

[4] Darekar M. S., Praveen B. M., (2022), Synthesis and characterization of nanoparticles ofsemiconducting metal sulphide and their application. Phys. Scr. 97: 065805. https://doi.org/10.1088/1402-4896/ac698f

[5] Darekar M. S., Praveen B. M., (2023), High photosensitivity nanocrystalline p-Cu2S/n-FTO heterojunction photodetectors prepared by dip coating method. J. Modern Nanotechnol. 3. DOI:10.53964/jmn.2023001 https://doi.org/10.53964/jmn.2023001

[6] Darekar M. S., Praveen B. M., (2023), Effects of heat treatment in air atmosphere on dip coating deposited CdS thin films for photo sensor applications. J. Modern Nanotechnol. 3. 2-9. https://doi.org/10.53964/jmn.2023002

[7] Bangal M., Ashtaputre S., Marathe S., Ethiraj A., Hebalkar N., Gosavi S. W., Urban J., Kulkarni S. K., (2005), Semiconducting nanoparticles. Springer, Hyperfine Interact. 160: 81-94. https://doi.org/10.1007/s10751-005-9151-y

[8] Azari B., Pourahmad A., Sadeghi B., Mokhtary M., Preparation and photocatalytic study of SiO2 /CuS coreshell nanomaterial for degradation of methylene blue dye. Nanoscale. 6:103-114.

[9] Sandroff C. J., Hwang D. M., Chung W. M., (1986), Carrier confinement and special crystallite dimensions in layered semiconductor colloids. Phys. Rev. B33: 5953-5958. https://doi.org/10.1103/PhysRevB.33.5953

[10] Dag I., Lifshitz E., (1996), Dynamics of recombination processes in PbI2 nanocrystal embedded in porous silica films. J. Phys. Chem. 100: 8962-8972. https://doi.org/10.1021/jp952863y
[11] Sandroff C. J., Kelty S. P., Hwang D. M., (1986), Clusters in solution: Growth and optical properties of layered semiconductors with hexagonal and honeycombed structures. J. Chem. Phys. 85: 5337-5341. https://doi.org/10.1063/1.451677
[12] Sabry N., Mohammed M. I., Yahia I. S., (2019), Optical analysis, optical limiting and electrical properties of novel PbI2/PVA polymeric nanocomposite films for electronic optoelectronic applications. Mater. Res. Express 6: 115339-115345. https://doi.org/10.1088/2053-1591/ab4c24
[13] Sheng C.-X., Zhai Y., Olejnik E., Zhang C., Sun D., Vardeny Z. V., (2015), Laser action and Photoexcitations dynamics in PbI2 films. Opt. Mater. Express 5: 530-537. https://doi.org/10.1364/OME.5.000530
[14] Liu J., Sun Y., Zhou Y., Zhang C., Wang X., Wang L., Xiao M., (2019), Few Layer PbI2 nanoparticle: A 2D semiconductor with lateral quantum confinement. J. Phys. Chem. Lett. 10: 7863-7869. https://doi.org/10.1021/acs.jpclett.9b03009
[15] Popov G., Mattinen M., Hatanpaa T., Vehkamaki M., Kemell M., Mizohata K., Raisanen J., Ritala M., Leskela M., (2019), Atomic layer deposition of PbI2 thin films. Chem. Mater. 31: 1101-1109. https://doi.org/10.1021/acs.chemmater.8b04969
[16] Shkir M., Yahia I. S., Ganesh V., Bitla Y., Ashraf I. M., Kaushik A., AlFaify S., (2018), A facile synthesis of Au-nanoparticles decorated PbI2 single crystalline nanosheets for optoelectronic device applications. Sci. Rep. 8: 13806-13811. https://doi.org/10.1038/s41598-018-32038-5
[17] Schluter I. CH., Schluter M., (1974), Electronic structure and optical properties of PbI2. Phys. Rev. B. 9: 1652-1656.
[18] Gahviller C., Harbecke G., (1969), Excitonic effects in the electro reflectance of lead iodide. Phys. Rev. 185: 1141-1147. https://doi.org/10.1103/PhysRev.185.1141
[19] Harbeche G., Tosatti E., (1975), Root Cause Analysis Rev. 36: 40-45.
[20] Minder R., Ottaviani G., Canali C., (1976), Charge transport in layer semiconductors. J. Phys. Chem. Solids 37: 417-424. https://doi.org/10.1016/0022-3697(76)90023-8
[21] Manfredotti C., Murri R., Quirini A., Vasanelli L., (1977), Proc. 1976 IEEE Nuclear Science Symposium February.
[22] Shkir M., AlFaify S., (2019), Effect of Gd3+ doping on structural, morphological, optical, dielectric, and nonlinear optical properties of high-quality PbI2 thin films for optoelectronic applications. J. Mater. 34: 2765-2774. https://doi.org/10.1557/jmr.2019.121
[23] Sengupta A., Mandal K. C., Zhang J. Z., (2000), Ultrafast electronic relaxation dynamics in layered Iodide semiconductors: A comparative study of colloidal BiI3 and PbI2 nanoparticles. J. Phys. Chem. B. 104: 9396-9403. https://doi.org/10.1021/jp000980+
[24] Mohammed S. I., Ahmed N. M., Al-Douri Y., Hashim U., (2014), Structural properties of PbI2 thin film. Adv. Mater. Res. 879: 175-179. https://doi.org/10.4028/www.scientific.net/AMR.879.175
[25] Nozue Y., Tang Z. K., Goto T., (1990), Excitons in PbI2 clusters incorporated into zeolite cages. Solid State Commun. 73: 531-534. https://doi.org/10.1016/0038-1098(90)91043-G
[26] Kaviyarasu K., Sajan D., Selvakumar M. S., Augustine Thomas S., Prem Anand D., (2012), A facile hydrothermal route to synthesize novel PbI2 nanorods. J. Phys. Chem. Solids 73: 1396-1400. https://doi.org/10.1016/j.jpcs.2012.06.005
[27] Shkir M., Yahia I. S., AlFaify S., Abutalib M. M., Muhammad S., (2016), Facile synthesis of lead iodide nanostructures by microwave irradiation technique and their structural, morphological, photoluminescence and dielectric studies. J. Mol. Struct. 1110: 83-90. https://doi.org/10.1016/j.molstruc.2016.01.014
[28] Ngqoloda S., Arendse C. J., Muller T. F., Magubane S. S., Oliphant C. J., (2020), Controlled deposition of Lead Iodide and Lead Chloride thin films by low-pressure chemical vapor deposition. Coat. 10: 1208-1212. https://doi.org/10.3390/coatings10121208
[29] Ghosh T., Bandyopadhyay S., Roy K. K., Kar S., Lahiri A. K., Maiti A. K., Goswami K., (2008), Optical and structural properties of lead iodide thin films prepared by vacuum evaporation method. Cryst. Res. Technol. 43: 959-963. https://doi.org/10.1002/crat.200811160
[30] Liang Y., Yao Y., Zhang X., Hsu W.-L., Gong Y., Shin J., Takeuchi I., (2016), Fabrication of organic-inorganic perovskite thin films for planar solar cells via pulsed laser deposition. AIP Adv. 6: 015001-015006. https://doi.org/10.1063/1.4939621
[31] Li W., Yang J., Jiang Q., Li R., Zhao L., (2018), Electrochemical deposition of PbI2 for perovskite solar cells. Sol. Energy. 159: 300-305. https://doi.org/10.1016/j.solener.2017.10.077
[32] Fornaro L., Saucedo E., Mussio L., Yerman L., Ma X., Burger A., (2001), Lead iodide film deposition and characterization. Nuclear Inst. Methods in Phy. Res. A. 458: 406-412. https://doi.org/10.1016/S0168-9002(00)00933-5
[33] Acuna D., Krishnan B., Shaji S., Sepulveda S., Menchaca J. L., (2016), Growth and properties of lead iodide thin films by spin coating. Bull. Mater. Sci. 39: 1453-1460. https://doi.org/10.1007/s12034-016-1282-z
[34] Condeles J. F., Mulato M., (2011), Influence of solution rate and substrate temperature on the properties of lead iodide films deposited by spray pyrolysis. J. Mater. Sci. 46: 1462-1468. https://doi.org/10.1007/s10853-010-4947-9
[35] Nikam C. P., Gosavi S. R., (2014), Characterization of nanocrystalline CdS thin films deposited on FTO by CBD for photo sensor applications. Adv. Nat. Appl. Sci. 5: 267-272.
[36] Manjulavalli T. E., Kannan A. G., (2015), Effects of deposition time on structural, optical and electrical properties of chemically deposited Cu2S thin films. Int. J. Chemtech. Res. 8: 607-616.
[37] Khimani A. J., Chaki S. H., Malek T. J., Tailor J. P., Chauhan S. M., Deshpande M. P., (2018), Cadmium Sulphide (CdS) thin films deposited by chemical bath deposition (CBD) and dip coating techniques: A comparative study. Mater. Res. Express 5: 036406-036411. https://doi.org/10.1088/2053-1591/aab28d
[38] Okorie O., Buba A., Ramalan A., (2017), Optical and dielectric properties of cadmium sulphide thin film grown using chemical bath deposition technique. IOSR: J. Appl. Phys. 9: 82-89.
[39] Yücel E., Kahraman S., Güder H., (2015), Effects of different annealing atmospheres on the properties of cadmium sulfide thin films. Mater. Res. Bull. 68: 227-233.

https://doi.org/10.1016/j.materresbull.2015.03.067
[40] Mahdi M. A., Kasem S. J., Hassen J. J., Swadi A. A., A1-Ani S. K. J., (2009), Structural and optical properties of chemical deposition CdS thin films. Int. J. Nanoelectron. Mater. 2: 163-172.
[41] Chowdhury R. I., Hossen M. A., Mustafa G., Hussain S., Rahman S. N., Farhad S. F., Murata K., Tambo T., Islam A. B., (2010), Characterization of chemically deposited cadmium sulfide thin films. Int. J. Mod. Phys. B. 24: 5901-5911. https://doi.org/10.1142/S0217979210055147
[42] Ismail R. A., Al Samarai A. M., Muhammed A. M., (2019), High-performance nanostructured p-Cu2S/n-Siphotodetector prepared by chemical bath deposition technique. J. Mater. Sci. Mater. Electron. 30: 11807-11818. https://doi.org/10.1007/s10854-019-01554-z
[43] Al-Taay H. F., (2017), Preparation and characterization of chemical bath deposition synthesis of CdS nanocrystalline thin films. Iraqi J. Sci. 58: 454-461. https://doi.org/10.24996/ijs.2017.58.1C.9
[44] More P., Dhanayat S., Gattu K., Mahajan S., Upadhye D., Sharma R., (2016), Annealing effect on Cu2S thin films prepared by chemical bath deposition. AIP, Conf. Proc. 1728: 020489-020495. https://doi.org/10.1063/1.4946540
[45] Patil M., Sharma D., Dive A., Mahajan S., Sharma R., (2018), Synthesis and characterization of Cu2S thin film deposited by chemical bath deposition method. Procedia Manuf. 20: 505-508. https://doi.org/10.1016/j.promfg.2018.02.075
[46] Henglein A., (1989), Small-particle research: Physiochemical properties of extremely small colloidal metal and semiconductor particles. Chem. Rev. 89: 1861-1873. https://doi.org/10.1021/cr00098a010
[47] Rahdar A., (2012), Effect of 1-Thioglycerol as capping agent on ZnS nanoparticles: Structural and optical characterization. Int. J. Sci. Eng. Investig. 1: 32-38. https://doi.org/10.1186/2193-8865-3-10
[48] Brus L. E., (1983), A simple model for the ionization potential, electron affinity, and aqueous redox potentials of small semiconductor crystallites. J. Chem. Phys. 79: 5566-5571. https://doi.org/10.1063/1.445676
[49] Brus L. E., (1984), Electron-electron and electron hole interactions in small semiconductor crystallites: The size dependence of the lowest excited electronic state. J. Chem. Phys. 80: 4403-4409. https://doi.org/10.1063/1.447218
[50] Suresh S. R., (2013), Studies on the dielectric properties of CdS nanoparticles. Appl. Nanosci. 4: 325-329. https://doi.org/10.1007/s13204-013-0209-x
[51] Sengupta A., Jiang B., Mandal K. C., Zhang J. Z., (1999), Ultrafast electronic relaxation dynamics in PbI2 semiconductor colloidal nanoparticles: A femtosecond transient absorption study. J. Phys. Chem. B. 103: 3128-3137. https://doi.org/10.1021/jp9842345
[52] Ekimov A. I., Efros A. L., Ivanov M. G., Onushchenko A. A., Shumilov S. K., (1985), Quantum size effect in semiconductor microcrystals. Solid State Commun. 56: 921-924. https://doi.org/10.1016/S0038-1098(85)80025-9
[53] Bawendi M. G., Kortan A. R., Steigerwald M. L., Brus L. E., (1989), X-ray structural characterization of larger CdSe semiconductor clusters. J. Chem. Phys. 91: 7282-7286. https://doi.org/10.1063/1.457295
[54] Vogel W., Urban J., Kundu M., Kulkarni S. K., (1997), Sphalerite-wurtzite intermidiates in nanocrystalline CdS. Langmuir. 13: 827-832. https://doi.org/10.1021/la960426k
[55] Lifshitz E., Yassen M., Bykov L., Dag I., Chaim R., (1994), Nanometer-sized particles of Lead Iodide embedded in silica films. J. Phys. Chem. 98: 1459-1463. https://doi.org/10.1021/j100056a015
[56] Darekar M. S., Praveen B. M., (2023), Hyperfine splitting and ferromagnetism in CdS : Mn nanoparticles for optoelectronic device applications. J. Semicond. (In Press).
[57] Mourdikoudis S., Pallares R. M., Thanh N. T. K., (2018), Characterization techniques for nanoparticles: comparison and complementarity upon studying nanoparticle properties. R. Soc. Chem. 10: 12871-12934. https://doi.org/10.1039/C8NR02278J